ELSEVIER

Significance of Shrinkage-Induced Clamping Pressure in Fiber-Matrix Bonding in Cementitious Composite Materials

Henrik Stang
Department of Structural Engineering, Technical University of Denmark, Lyngby

The present paper assesses the significance of shrinkage-induced clamping pressure in fiber-matrix bonding mechanisms in cementitious composite materials. The paper contains a description of an experimental setup that allows measurement of the clamping pressure, which develops on an elastic inhomogeneity embedded in a matrix consisting of a cementitious material undergoing shrinkage during hydration (autogenous shrinkage). Furthermore, the paper presents the analysis necessary to perform an interpretation of the experimental results and to determine the clamping pressure acting on any elastic inhomogeneity embedded in the same cementitious matrix material. Fiber-shaped inhomogeneities are of special interest in cementitious composite material systems, and results are presented for the development of clamping pressure on three typical fiber types in two typical cement pastes used in high performance cementitious composite materials. Assuming a Coulomb type of friction on the fiber-matrix interface and using typical values for the frictional coefficient, it is shown that the shrinkage-induced clamping pressure could be one of the most important factors determining the frictional stresses observed on debonded fiber-matrix interfaces during pullout. ADVANCED CEMENT BASED MATERIALS 1996, 4, 106–115

KEY WORDS: Bond, Cement, Composite materials, Concrete, Eigenstress, Fiber reinforcement, Interface, Shrinkage

In fiber reinforced brittle matrix composites, the fiber-matrix interface properties are very important factors in determining of the overall mechanical properties of the composite material. In short fiber composites interface properties play an important role in governing the fiber debonding and pull-out process that controls the stress-crack opening relationship. This relationship is considered the key to describing the nonlinear behavior of such materials [1]. Anything from a slight modification of the matrix properties to the creation of very ductile pseudostrain hardening materials can be obtained by varying the interface parameters. In continuous fiber systems, the interface properties primarily control the crack width and first crack strength, and anything from ductile to perfectly brittle behavior in tension can be obtained by varying the interface parameters. These considerations hold for brittle matrix composites in general and for cement based composite materials in particular.

Due to the importance of the fiber-matrix bond, a great number of analytical models and experimental results have been presented in the literature over the years in an attempt to quantify the bond between fiber and matrix in different fiber-matrix systems. In cementitious matrix composite systems, emphasis has been placed primarily on frictional effects on the debonded interface. Adhesive effects on the bonded interface have also been proposed as an important energy consuming mechanism active on the fiber-matrix interface during debonding.

In ceramic matrix composite systems where the composite is manufactured under high temperature and where the service life is often characterized by large temperature variations, it is well known that eigenstresses are introduced and a certain clamping effect on the fiber arises due to the different thermal expansion coefficients of the fiber and matrix material. Consequently, this clamping effect is often included in analytical models and in interpretation of experimental results [2]. Usually, this is done by assuming a Coulomb type of friction on the debonded interface:

$$|\tau| = \mu p \tag{1}$$

where τ is the frictional shear stresses, μ is the coefficient of friction, and p is the magnitude of the compres-

Address correspondence to: Henrik Stang, Department of Structural Engineering, Technical University of Denmark, Building 118, DK-2800 Lyngby, Denmark.
Received August 25, 1995; Accepted July 30, 1996

ISSN 1065-7355/96/$15.00
PII S1065-7355(96)00075-2

sive contact stress—the clamping pressure—acting on the fiber-matrix interface.

The same situation arises in cementitious materials due to the shrinkage of the matrix during the hydration process. Furthermore, there is presently some evidence that a Coulomb type of friction is governing the shear stresses on the debonded interface in cementitious composite systems (for example, refs. 3 and 4). However, rarely is shrinkage explicitly included in models for fiber-matrix bonding or debonding in cementitious materials. This is due to the fact that even though the different types of shrinkage, autogenous as well as drying out, can be measured fairly easily, the shrinkage takes place at the same time as significant changes in the elastic and viscoelastic properties of the matrix material. Thus, it is not at all evident how a calculation of the clamping pressure should be performed.

The significance of the clamping pressure and related initial stress states in the overall behavior of concrete was pointed out by Acker et al. [5]. It is suggested by Acker et al. that aggregates in concrete may be used as pressure sensors in a suitable experimental approach, and measurements on a cylindrical sensor embedded in the middle of a disc of mortar are presented. Recently, linear elastic analytical solutions for eigenstresses caused by expanding or shrinking aggregates and pastes along with experimental observations of cracking patterns around aggregates caused by these eigenstresses were presented by Goltermann [6] and [7]. Furthermore, an attempt to predict the magnitude of eigenstresses around aggregates caused by matrix shrinkage was made by Dela [8] using linear elastic solutions and a stepwise calculation taking into account the change in stiffness but disregarding the relaxation. Finally, the work by Kim et al. and Zhou et al. should be mentioned [9–11]. In this work, the interfacial parameters—including clamping pressure and coefficient of friction—are determined from available experimental fiber pullout data using a model for fiber pullout that takes clamping pressure into account.

This paper presents a technique for measuring the clamping pressure acting on inhomogeneities and related to autogenous shrinkage of the cementitious paste. This technique is based on the use of a mercury thermometer as a pressure sensor. The mercury container of an ordinary laboratory thermometer is shown to be a very simple and sufficiently accurate pressure sensor that can monitor the development of the contact stresses.

In the interpretation of the test results, the pressure sensor is modeled as an equivalent homogeneous elastic ellipsoidal inhomogeneity and the surrounding cementitious matrix is modeled as an infinite elastic medium. This modeling allows for the use of the well-known Eshelby solution [12] and introduces the definition of an effective shrinkage that can be used in the estimation of contact stresses on other inhomogeneities than the pressure sensor, such as fibers or aggregates. This estimation is carried out and the results for clamping pressure on different typical fiber types used in cementitious composites are derived. Assuming that a Coulomb type of friction is governing the frictional shear stress acting on the debonded fiber-matrix interface in cementitious composites, the shrinkage-related frictional shear stress can be estimated and compared with typical values for frictional shear stress observed in, for example, pullout experiments. Thus, the significance of the shrinkage-related frictional shear stresses can be assessed. Preliminary results using the proposed method were first published in ref. 13. The present paper gives the complete background for the experimental work, and the theoretical analysis and supplementary data are presented.

The Experimental Setup

The basic idea is to use a laboratory mercury thermometer as a pressure sensor for the determination of shrinkage-related clamping pressure. A standard mercury thermometer consists of a glass container filled with mercury. The container is connected to a capillary class tube. Volume changes in the mercury due to temperature changes are then detectable as changes in position of the mercury surface in the capillary tube. Obviously, volume changes of the glass container due to mechanical action, for example, external hydrostatic pressure, can also be detected as changes in mercury surface position. Simultaneous changes in pressure and temperature can be measured if a second pressure-independent temperature measuring device, such as an electrical thermocouple, is introduced in the system.

For the present experiments, a laboratory thermometer with a temperature range of 50 °C and an accuracy of 1/10 °C was chosen. The outer glass tube that was connected to the mercury container and that was protecting the capillary tube was removed by cutting close to the connection to the mercury container. Finally, the temperature scale that originally was connected to the outer protecting tube was fixed to the capillary tube. The different parts of the measuring device are shown in Figure 1.

The measuring device was calibrated for hydrostatic pressure in pressurized air in a small pressure chamber designed for this purpose. This resulted in the calibration factor α (MPa/°C) relating apparent temperature change to hydrostatic pressure. Furthermore, the amount of mercury in the capillary tube was measured by weighing the tube with and without mercury and the calibration factor β (g/°C) was determined relating

Advn Cem Bas Mat
1996;4:106–115

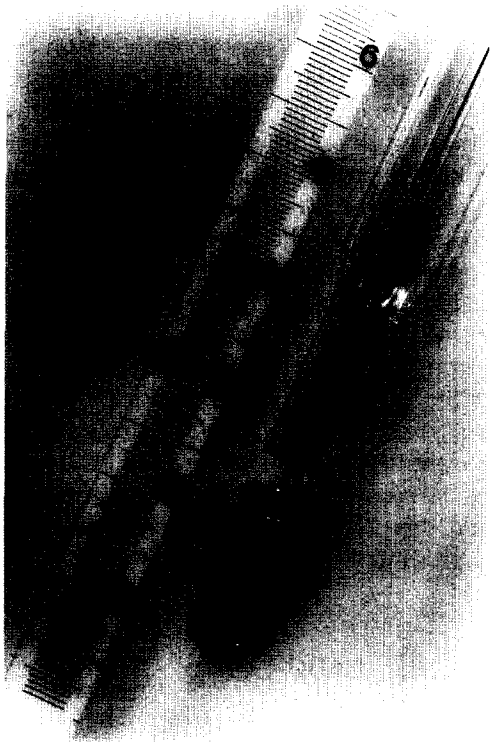

FIGURE 1. Photograph showing the different parts of the mercury thermometer used as a pressure sensor in the experimental investigations.

apparent temperature change to mass of mercury. After having determined the total volume of the mercury container υ (glass and mercury), one can determine the equivalent compression modulus (or bulk modulus) κ^e from the formula

$$\kappa^e = \frac{\alpha\gamma_{hg}}{\beta}\upsilon \tag{2}$$

where γ_{hg} is the density of mercury and where the bulk modulus κ according to the theory of elasticity is defined as

$$\kappa = \frac{\sigma_{ii}}{3\varepsilon_{ii}} \tag{3}$$

The experimentally determined equivalent compression modulus κ^e can be compared with a linear elastic solution for the equivalent compression modulus κ^{e*}. Such a solution is obtained by modeling the mercury container as a thin axis-symmetric ellipsoidal elastic shell with wall thickness h, aspect ratio a/b (where a is the length of the half-axis in the direction of symmetry), Young's modulus E^s, and Poisson's ratio ν^s. It can be shown that [14]

$$\kappa^{e*} = \frac{2E^s h}{3bI} \tag{4}$$

where I is a function of a/b and ν^s.

In the case of a spherical shell and an infinitely long cylindrical shell, I is given by

$$I = (1 - \nu^s) \text{ for } a = b \tag{5}$$

and

$$I \to \frac{3\pi}{16}\left(\frac{5}{2} - 2\nu^s\right) \text{ for } \frac{a}{b} \to \infty. \tag{6}$$

For the Poisson's ratio and aspect ratio considered here, I will be very close to 1.

After calibration, the sensor is cast into the center of a volume of cement paste contained in a cylindrical steel can. The volume has a diameter of 100 mm and a height of 60 mm. Next to the pressure sensor, two electrical thermocouples are placed allowing for pressure-independent temperature measurements during the hydration process as well as during long-term testing. Immediately after casting, the cement paste is covered with a thin layer of oil protecting the paste from water evaporation. Thus, the cementitious matrix experiences only autogenous shrinkage and the temperature variation connected with the hydration process. The experimental setup is shown in Figure 2.

The basic observations consist of observed temperature differences ΔT between the modified mercury ther-

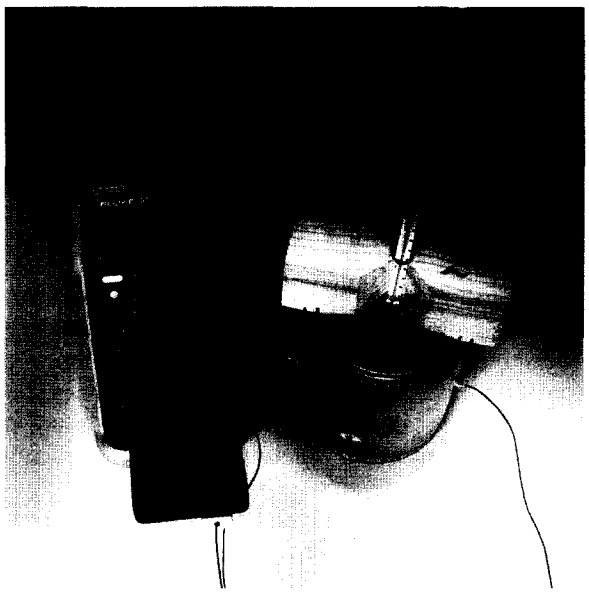

FIGURE 2. Photograph showing the experimental setup, the steel container, the stripped thermometer, and the thermocouple module.

mometer and the average of the two electrical thermocouples observed over a period of time t where $t = 0$ corresponds to the time of casting of the cement paste in the steel container (less than 1 hour after mixing). The observations of ΔT should, of course, be corrected for any difference in temperature between the thermometer and the thermocouple reading at $t = 0$. Through the calibration factor α, the observed ΔT can readily be translated to an equivalent hydrostatic stress state σ^e_{hyd} in the equivalent elastic inhomogeneity:

$$\sigma^e_{hyd}(t) = \alpha(\Delta T(t) - \Delta T(t = 0)). \tag{7}$$

The Analysis and Interpretation

The analysis is based on the solution for an isotropic, linear elastic ellipsoidal inhomogeneity embedded in an isotropic, linear elastic infinite medium undergoing shrinkage. The solution for this problem can be obtained following Eshelby's original superposition scheme [12] with a homogeneous infinite medium and an inclusion undergoing a stress-free strain. The only difference between Eshelby's original and the present calculation is that instead of loading the infinite medium with a homogeneous stress and strain field related by the stiffness of the infinite medium, the entire infinite medium is assumed to undergo a stress-free strain ε^s_{ij}.

It can be shown that using the standard index notation the solution for the stress and strain in the inhomogeneity takes the following form,

$$\varepsilon^i_{ij} = G_{ijkl}\, \varepsilon^s_{kl} \tag{8}$$

$$\sigma^i_{ij} = H_{ijkl}\, \varepsilon^s_{kl} \tag{9}$$

where σ^i_{ij} and ε^i_{ij} is stress and strain in the inhomogeneity and where ε^s_{ij} is the free matrix shrinkage strain state given by

$$\varepsilon^s_{ij} = \delta_{ij}\, \varepsilon^s \tag{10}$$

where ε^s is the free linear matrix shrinkage strain and δ_{ij} is Kronecker's delta.

The fourth-order tensors G_{ijkl} and H_{ijkl} are given by the following expressions:

$$G_{ijkl} = [I_{ijpq} + P^i_{ijmn}\, (L^i_{mnpq} - L^m_{mnpq})]^{-1}\, (I_{pqkl} - S^i_{pqkl}) \tag{11}$$

and

$$H_{ijkl} = L^i_{ijmn}\, G_{mnkl} \tag{12}$$

with

$$P^i_{ijkl} = S^i_{\text{ijmn}}\, M^m_{mnkl} \tag{13}$$

where I_{ijkl} is the fourth-order unit tensor and S^i_{ijkl} is the Eshelby S-tensor [12] for the inclusion. In ref. 12, the full analytical solution for the components of the S-tensor are available. The tensors L^i_{ijkl} and L^m_{ijkl} are the stiffness tensors for the inhomogeneity and the infinite medium, respectively, whereas the flexibility tensor for the infinite medium is denoted M^m_{ijkl}. Thus, the stress and strain fields in the infinite medium are related through:

$$\sigma^m_{ij} = L^m_{ijkl}\, \varepsilon^m_{kl} \tag{14}$$

or

$$\varepsilon^m_{ij} = M^m_{ijkl}\, \sigma^m_{kl} \tag{15}$$

while the stress and strain in the inhomogeneity are related through equivalent relations with superscript m substituted with superscript i. The stiffness tensors can be expressed in terms of two independent elastic engineering constants, Young's modulus E and Poisson's ratio ν or bulk modulus κ and Poisson's ratio ν.

For any given stress state in the inhomogeneity σ^i_{ij} with the hydrostatic part σ^i_{hyd}, the corresponding free shrinkage in the infinite medium can be determined according to

$$\varepsilon^s = \frac{\sigma^i_{ii}/3}{h} = \frac{\sigma^i_{hyd}}{h} \tag{16}$$

where

$$h = \frac{H_{iikk}}{3}. \tag{17}$$

If, on the other hand, the shrinkage is known, the surface stress vector p_i on the surface of the inhomogeneity can be determined according to

$$p_i = \sigma^i_{ij} n_j \tag{18}$$

where n_i is the outward unit normal vector to the surface of the inhomogeneity. The vector p_i can easily be determined in every point on the surface, because the stress state σ^i_{ij}, determined through eq 9, is homogeneous in the inhomogeneity as shown by Eshelby [12].

The equations derived above hold for any ellipsoidal inhomogeneity. However, two special cases are of interest here: the spherical inhomogeneity (corresponding to a rounded aggregate) and the cylindrical inhomogeneity with a circular cross section (corresponding to a fiber with high aspect ratio).

In the case of a spherical inhomogeneity, all the fourth-order tensors including the G- and H-tensors are isotropic. Therefore, the stress state σ^i_{ij} is hydrostatic.

Advn Cem Bas Mat
1996;4:106–115

Thus, the vector p_i is always perpendicular to the surface of the sphere, and the magnitude p is given by

$$p = |p_i| = |\sigma_{11}^i| = |\sigma_{22}^i| = |\sigma_{33}^i| \tag{19}$$

which can be expressed as

$$p(\varepsilon^s) = \frac{2E^m}{(1+\nu^m) + 2\frac{E^m}{E^i}(1-2\nu^i)} |\varepsilon^s|. \tag{20}$$

In the case of a cylindrical inhomogeneity with circular cross section, the G- and H-tensors are transversely isotropic and σ_{ij}^i is hydrostatic in planes perpendicular to the axis of symmetry with no shear stresses in the direction of the axis of symmetry. Thus, p_i is always perpendicular to the cylindrical surface of the inhomogeneity. If the x_3-axis is assumed to be parallel to the axis of symmetry, we have

$$p = |p_i| = |\sigma_{11}^i| = |\sigma_{22}^i| \tag{21}$$

which through some lengthy calculations can be expressed as

$$p(\varepsilon^s) = \frac{E^m}{\frac{1+\nu^m}{1+\nu^i} + \frac{E^m}{E^i}(1-2\nu^i)} |\varepsilon^s|. \tag{22}$$

To utilize the above analysis in the interpretation of the experimental results described in the previous section, we define the concept of *effective shrinkage* $\varepsilon^{s,e}$, which is a function of time defined by

$$\varepsilon^{s,e}(t) = \frac{\sigma_{hyd}^e(t)}{h(t)} \tag{23}$$

where $\sigma_{hyd}^e(t)$ is obtained directly from the experiment. Calculation of $h(t)$ requires knowledge of the elastic constants for the cement paste as functions of time as well as the equivalent elastic constants of the pressure sensor. As shown in the previous section, the equivalent bulk modulus for the sensor can be determined, but the equivalent Poisson's ratio is not measured directly. However, it is shown in the next section that $h(t)$ is relatively insensitive to changes in equivalent Poisson's ratio; in fact, if the sensor is spherical in shape, then h is independent of Poisson's ratio. Equation 23 defines the effective shrinkage as the shrinkage that in a linear elastic system, would introduce the correct stress state in an embedded equivalent inhomogeneity if the matrix shrinkage took place momentarily at time t.

The effective shrinkage at time t can be used to estimate the clamping stress acting on different inhomogeneities embedded in the same cementitious paste at the same time. This can be done through eq 20 and 22, using the appropriate values for the elastic constants of the inhomogeneity. Thus, the development in clamping pressure can be evaluated through

$$p(\varepsilon^s) = p(\varepsilon^{s,e}(t)). \tag{24}$$

Results and Discussion

Four tests were carried out with two different cementitious matrices. One matrix consisted of cement paste with a water:cement (w:c) ratio of 0.3. The other mix contained 10% microsilica, also with a w:c ratio of 0.3. In both mixes, a super-plastizicer was used to allow easy casting of the mix in the container with the pressure sensor and the thermocouples mounted. The contents of the mixes are summarized in Table 1. The mixing procedure described in ref. 8 was used also in the present investigation.

The mixes correspond well with typical paste mixes used in high quality concretes and cementitious composites. Furthermore, the mechanical properties of the two mixes—Young's modulus, tensile strength as well as fracture toughness—were investigated in detail as functions of time by Dela [8]. Young's modulus as function of time for the two mixes was determined from least square curve fitting using a logarithmic expression. For the 0% microsilica mix, the following function was used

$$E_0^m = 500 \ln\left(\frac{t_{30} - 0.23}{t_{30}}\right) + 24.6 \text{ [GPa]} \quad t_{30} > 8 \text{ h} \tag{25}$$

while

$$E_{10}^m = 645 \ln\left(\frac{t_{30} - 0.20}{t_{30}}\right) + 25.9 \text{ [GPa]} \quad t_{30} > 8 \text{ h} \tag{26}$$

was used in the case of the 10% microsilica mix. In the

TABLE 1. Composition of the two cement paste mixes investigated

Component		0% Microsilica	10% Microsilica
White portland cement	[g/l]	1606	1498
Microsilica slurry (water 50.2%)	[g/l]	—	300.9
Super-plasticizer (water 70.0%)	[g/l]	56.21	57.69
Demineralized water	[g/l]	442.5	258.1

Note: The mixing procedure is described in detail in ref. 8.

above equations, t_{30} denotes time in hours at 30 °C. The current investigation was carried out at 20 °C, and the time scale was converted according to ref. 15

$$t_{20} = 1.6t_{30}. \tag{27}$$

The Poisson's ratio was assumed to be constant (0.20) in time.

The obtained results for calibration factors and effective bulk moduli for the four different thermometers used are summarized in Table 2. In Table 2, the measured bulk moduli are compared with the values calculated from the linear elastic shell solution. As shown, the measured and calculated values for the bulk modulus, κ^e and κ^{e*}, are in reasonably good agreement. In all calculations presented here, κ^e is used. The sensors 1 and 2 are used in the mix containing 10% microsilica, while the sensors 3 and 4 are used in the paste with no microsilica.

In Figure 3, the development in equivalent hydrostatic stress σ^e_{hyd} determined according to eq 7 is shown for the four different mixes. Figure 3 clearly shows that there is a significant difference between the two pastes. A much higher hydrostatic stress develops in the sensors embedded in microsilica paste. Furthermore, the hydrostatic stress keeps rising in the microsilica paste while it rises and then after approximately 50 hours it drops to an almost constant level in the paste without microsilica. The test with sensor 1 was carried out first, while the three other tests were carried out over the same period of time. Apparently, there is some difficulty with reproducing the microsilica paste results, even though the trend for sensor 1 and 2 is the same. This could be due either to influence from the laboratory environment or to difficulties related to dispersion of the microsilica. However, after 500 hours, the tests with sensor 1 and 2 produced very similar results. Furthermore, it should be noted that when tests are carried out with the same batch over the same period of time (sensor 3 and 4) the results are very reliable.

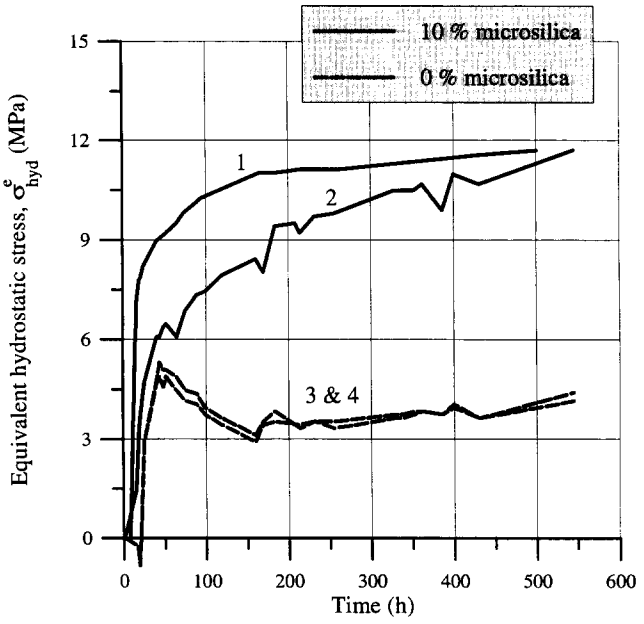

FIGURE 3. Development in equivalent hydrostatic stress σ^e_{hyd} in the pressure sensors 1, 2, 3 and 4.

Knowing Young's modulus for the paste as a function of time and assuming a constant Poisson's ratio of 0.2, and having determined the aspect ratio $l = a/b$ (see Table 2) and the equivalent bulk modulus of the pressure sensor, $h(t)$ can be calculated. Only the equivalent Poisson's ratio ν^e for the pressure sensor is not known. A sensitivity analysis is carried out based on matrix properties corresponding to the microsilica matrix at t = 500 hours. The results of the sensitivity analysis is shown in Figure 4. The sensitivity analysis is carried out for three different aspect ratios l of the sensor. The spherical sensor l = 1.0 is unaffected by ν^e; the typical sensor geometry, l = 2.2, shows a 5% variation in h for all possible values of ν^e; and a very long sensor shows a 15% variation in the values of h. For all practical purposes, we can with sufficient accuracy assume ν^e = 0.2.

Using eqs 23 and 24, we can calculate the effective

TABLE 2. Calibration factors and dimensions for the pressure sensors along with the calculated equivalent compression moduli κ^e and κ^{e*} for the sensors used in the present investigation

Factors	Dimensions	Sensor 1	Sensor 2	Sensor 3	Sensor 4
α	MPa/°C	1.08	0.98	1.04	1.04
β	g/°C	$8.0\ 10^{-4}$	$8.0\ 10^{-4}$	$8.0\ 10^{-4}$	$8.0\ 10^{-4}$
υ	cm^3	0.52	0.51	0.50	0.60
κ^e	GPa	9.6	8.5	8.9	10.6
a	mm	8.5	7.7	8.4	8.5
b	mm	3.8	4.0	3.8	4.1
h	mm	0.7	0.7	0.7	0.7
I		1.08	1.03	1.08	1.06
κ^{e*}	GPa	8.5	8.5	8.5	8.1

Note: In all calculations, the following material constants were used: γ_{hg} = 13.6 g/cm^3, E^s = 75 GPa, ν^s = 0.2. The sensors 1 and 2 are used in the mix containing 10% microsilica, while the sensors 3 and 4 are used in the paste with no microsilica.

Advn Cem Bas Mat
1996;4:106–115

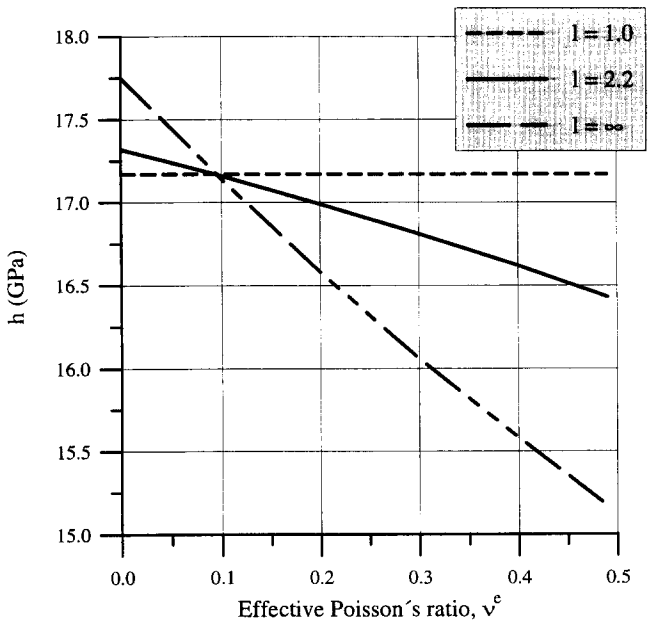

FIGURE 4. The shrinkage factor h as function of the undetermined equivalent Poisson's ratio ν^e for the sensor. Three different aspect ratios l are investigated: the typical sensor aspect ratio 2.2, the spherical sensor geometry (l = 1.0), and the very long sensor.

shrinkage $\varepsilon^{s,e}(t)$ and the magnitude of the clamping pressure acting on different types of fibers (and a typical aggregate) as functions of time. In Figures 5 and 6, the results are shown for the cement mix containing 0% and 10% microsilica, respectively. In Table 3, the elastic constants for the fibers and aggregate used in the calculations are shown together with values for the coefficient of friction found in the literature. Typical values for steel and carbon fibers as well as aggregate are used. With respect to the polypropylene fibers, it should be noted that these are often very anisotropic, especially the fibrillated fibers that are manufactured by cutting stretched polypropylene sheets. Thus, usually the transverse stiffness is low compared to the axial (which can easily reach values of about 10 GPa). The value of 1 GPa used in the present analysis should be considered a rough estimate. In Table 4, the mean value of the clamping pressure at 500 hours along with estimations of the Coulomb shear stresses acting on the fiber interface during fiber pullout in the two different pastes are shown together with typical results reported in the literature.

Not much data on coefficients of friction between different fibers and a cementitious matrix is available. From the work of Leung and Geng [4], a frictional coefficient of 0.125 for steel fiber in mortar can be deduced, relating *unilateral* clamping pressure to average friction. From the work of Pinchin and Tabor, values of 0.05–0.160 can be deduced—again for steel fibers in a cementitious paste. Finally, Kim et al. [11] determine coefficients of friction in the order of 0.08 for the same fiber-matrix systems. Consequently, values from 0.05 to 0.25 are used in Table 3 for steel fiber systems. No direct measurements of the frictional coefficient in carbon or polypropylene fiber systems are available in the literature. However, measurements of the friction between concrete and butyl sheets have been carried out [16] indicating values in the range of 0.45–0.75. Also, the frictional coefficient between polymeric materials and steel is known to be in the range of 0.3–0.5. Based on this knowledge, we assume the coefficient of friction between a soft polypropylene fiber and a cementitious

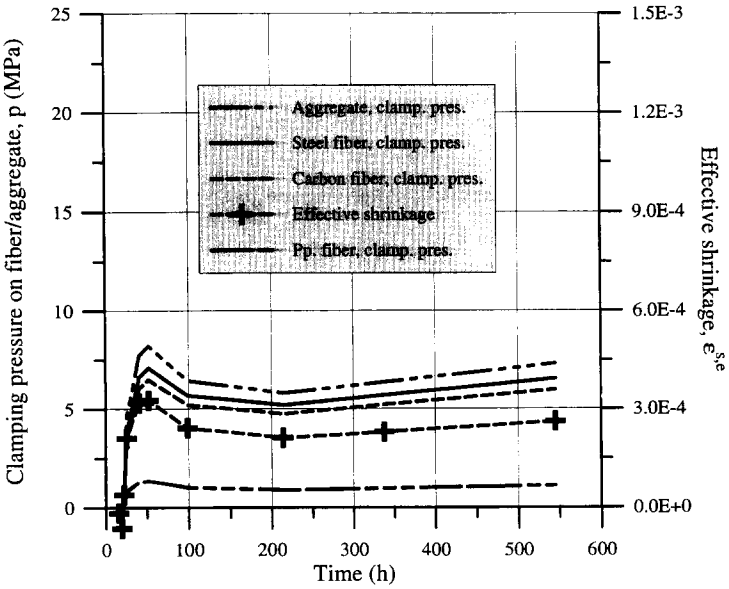

FIGURE 5. Development in calculated clamping pressure (clamp, pres.) for different inhomogeneities along with the calculated effective shrinkage in cement paste with 0% microsilica. The elastic constants for the inhomogeneities used in the calculation are summarized in Table 3. The curves are calculated on the basis of results obtained from sensor 3. Pp. = polypropylene.

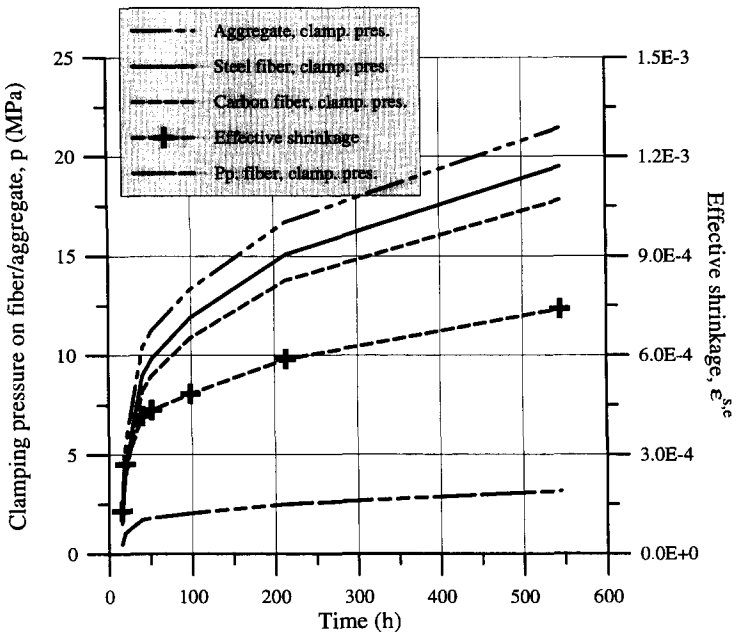

FIGURE 6. Development in calculated clamping pressure (clamp. pres.) for different inhomogeneities along with the calculated effective shrinkage in cement paste with 10% microsilica. The elastic constants for the inhomogeneities used in the calculation are summarized in Table 3. The curves are calculated on the basis of results obtained from sensor 2. Pp. = polypropylene.

matrix to be in the range of 0.3–0.5, whereas we assume the coefficient of friction in a carbon fiber system taking the hardness of the fiber into consideration is in the range of 0.05–0.1.

Looking at Figures 5 and 6, it is interesting to note that the effective shrinkage rises very quickly from t = 0 and reaches values from 3. 10^{-4} to 4. 10^{-4} in the first 25–40 hours depending on the paste (highest in the paste containing microsilica). After 50 hours, the effective shrinkage in the paste without microsilica drops to an almost constant level of about 2.0 10^{-4}–2.5 10^{-4}. In the paste with microsilica, the effective shrinkage continues to rise, however, with a much lower rate. Roughly speaking, the effective shrinkage doubles in the next 500 hours and reaches approximately 7. 10^{-4}. The free linear autogenous shrinkage has been measured by using a special technique developed by Mejlhede [17]. The free linear autogenous shrinkage for the mixes used in the present investigation was determined by Dela [8], using the technique developed by Mejlhede. For the paste without microsilica, a very rapid increase (within the first 20 hours at 30 °C) to a value of about 2. 10^{-3} is reported. After this time, practically no shrinkage takes place. For the paste with microsilica, the shrinkage reaches about 4. 10^{-3} after the first 20 hours, after which the shrinkage rate is significantly reduced. After about 500 hours at 30 °C, a shrinkage of 6. 10^{-3} is reached. It seems obvious from these observations that the effective shrinkage is related to the free autogenous shrinkage. It is also clear that there is a vast difference (one order of magnitude) between the magnitude of the observed free shrinkage and the effective shrinkage. This can be explained by the fact that a large part of the autogenous shrinkage takes place when the stiffness of the paste can be neglected. Furthermore, the relaxation seems to play an important role resulting in a drop in the effective shrinkage when the free shrinkage becomes constant (mix with no microsilica).

Furthermore, it is interesting to note that the calculated range of values for the frictional shear stresses correspond extremely well to corresponding values for bend or frictional stresses observed by many independent sources and reported in the literature (see refs. 13 and 18). Not only is the order of magnitude of the shear stresses correct but the variation of the magnitude of these from steel to carbon and polypropylene fibers is also correct. In ref. 13, frictional shear stresses in steel fiber systems from 0.43–4.9 MPa are reported, whereas average bond strength values (including adhesive as well as frictional stresses) in polypropylene fiber and carbon fibers systems of 0.45 MPa and 0.52–0.66 MPa, respectively, are reported. Finally, it should be noted that the prediction of clamping pressure developing around steel fibers corresponds very well with the (corrected) values for clamping pressure given in ref. 11.

TABLE 3. Elastic constants assumed to be associated with typical inhomogeneities and the frictional coefficents of the fiber-matrix interfaces

Inhomogeneity	E^i [GPa]	ν^i	μ
Steel fiber	210	0.3	0.05–0.25
Carbon fiber	240	0.2	0.05–0.1
Polypropylene fiber	1	0.4	0.3–0.5
Stone aggregate	54	0.2	—

Advn Cem Bas Mat
1996;4:106–115

TABLE 4. Predicted clamping pressure (mean of two predictions) and frictional shear stresses on fiber-matrix interfaces at $t = 500$ h in the pastes containing 0 and 10% microsilica

Inhomogeneity	p (MPa) 0% ms	p (MPa) 10% ms	τ (MPa) 0% ms	τ (MPa) 10% ms	τ (MPa) ref. 13
Steel fiber	6.4	19	0.3–1.6	1.0–4.8	0.43–4.9
Carbon fiber	5.9	17	0.3–0.6	0.9–1.7	0.45
Polypropylene fiber	1.1	3.1	0.3–0.6	0.9–1.6	0.52–0.66
Stone aggregate	7.1	21	—	—	—

Note: The table also summarizes values for the frictional shear stress reported in the literature. ms = microsilica.

It is also interesting that a clear distinction between microsilica paste and ordinary cement paste can be made in terms of frictional stresses at the interface. The present work suggests that a higher shear stress on debonded fiber-matrix interfaces can be achieved by introducing microsilica in the paste. Furthermore, a more favorable development of these shear stresses with time can be achieved.

It should be noted that the present analysis does not take into account the size effects that might come into play when the fiber diameters are small compared to the microstructure of the paste. Also, possible differences in the microstructure of the interfacial layers of different fiber types are neglected in the present analysis. It is well known that different fiber or aggregate types give rise to different characteristics of the interfacial layer in the cement paste (see ref. 19) depending on the chemical, physical, or geometrical characteristics of the inhomogeneity. Thus, it must be expected that the interfacial layer built around the glass pressure sensor in the present investigation is different from the layer that will be formed around a steel fiber. If the layer has a different stiffness and/or a different thickness, the clamping pressure will be affected.

Furthermore, interaction effects between fibers in cement composites or between fibers and aggregates in fiber concretes and mortars have not been taken into account. It is expected that these interaction effects will reduce the effective shrinkage experienced by each fiber or aggregate, because neighboring inhomogeneities will introduce constraints on the shrinkage deformation.

The effective shrinkage includes relaxation effects, because it is based on direct measurements of the clamping stresses. However, it is well known that long-term relaxation effects can be observed over much longer time spans than those used in the present investigation. Thus, care should be taken in extrapolating the present results over longer time spans.

Finally, in the present analysis, the coefficient of friction is considered a constant. This is probably a simplification. Chemical reactions are known to take place over time on different fibers, causing changes in the geometry of the fiber surface, typically increasing the roughness. These changes are likely to produce changes in (increase) the coefficient of friction.

Conclusions

The following conclusions can be drawn from the present work:

- The shrinkage-induced clamping pressure acting on aggregates and different fiber types embedded in two different cement pastes with and without microsilica has been estimated as a function of time over the first 500 hours. The estimation is based on direct measurement of the pressure developed in a simple pressure sensor embedded in the same matrix and a subsequent analysis based on Eshelby's solution for an ellipsoidal inhomogeneity embedded in an infinite matrix.
- Assuming a Coulomb frictional law on the fiber-matrix interface and using standard values for the frictional coefficient, frictional shear stresses on the debonded interface are estimated that are similar in magnitude to values reported in the literature describing fiber pullout tests. This suggests that matrix shrinkage and related clamping pressure might be an important mechanism to consider when investigating fiber-matrix bonding in cementitious composite systems.
- The method described in the present work provides an easy way of estimating clamping pressure and eigenstress states in cementitious composites systems. More work needs to be done to clarify effects related to size; presence of interfacial layers; and interaction between fibers, aggregates, and other inhomogeneities.

Acknowledgments

I thank Professor V.C. Li for the valuable discussions that initiated the present work, and I acknowledge the support from *NATO International Scientific Exchange Programs, Collaborative Research, grant No. 930023* for making the collaborative research possible.

Furthermore, I thank Helge Fredslund, Department of Structural Engineering, Technical University of Denmark (DTU), for his innovative assistance in the experimental work described here and graduate student Birgitte Dela, Building Materials Laboratory, DTU, for her help with carrying out a large part of the experiments.

Finally, I acknowledge Professor H. Møllmann, Department of Structural Engineering, DTU, for his kind help with the derivation of the solution for a linear elastic ellipsoidal shell.

References

1. Li, V.C.; Mihashi, H.; Alwan, J.; Brincker, R.; Horii, H.; Leung, C.; Stang, H.; Maalej, M.; Wu, H.C. In *High Performance Fiber Reinforced Cement Composites—Volume 2 (HPFRCC-95)*; Naaman, A.E.; Reinhardt, H.W., Eds.; University of Michigan: Ann Arbor, **1995,** pp 43–95.
2. Hashin, Z. *J. Appl. Mech.* **1983,** *50,* 481–505.
3. Pinchin, D.J.; Tabor, D. *J. Mater. Sci.* **1978,** *13,* 1261–1266.
4. Leung, C.K.Y.; Geng, Y. *Submitted for publication.*
5. Acker, P.; Boulay, C.; Rossi, P. *Cem. Concr. Res.* **1987,** *17,* 755–764.
6. Goltermann, P. *ACI Mater. J.* **1994,** *91,* 543–550.
7. Goltermann, P. *ACI Mater. J.* **1995,** *92,* 58–63.
8. Dela, B. *Shrinkage Cracking in High Strength Concrete. Master's Thesis;* Technical University of Denmark: Lyngby, **1994.** (In Danish)
9. Kim, J.-K.; Baillie, C.; Mai, Y.-W. *J. Mater. Sci.* **1991,** *27,* 3143–3154.
10. Zhou, L.-M.; Kim, J.-K.; Mai, Y.-W. *J. Mater. Sci.* **1992,** *27,* 3155–3166.
11. Kim, J.-K.; Zhou, L.-M.; Mai, Y.-W. *J. Mater. Sci.* **1993,** *28,* 3923–3930.
12. Eshelby, J.D. *Proc. R. Soc. Lond.* **1957,** *A241,* 376–396.
13. Bentur, A.; Banthia, N.; Baggott, R.; Hansen, W.; Katz, A.; Leung, C.K.Y.; Li, V.C.; Mobasher, B.; Naaman, A.E.; Robertson, R.; Soroushian, P.; Stang, H.; Taerwe, L.R. In *High Performance Fiber Reinforced Cement Composites—Volume 2 (HPFRCC-95)*; Naaman, A.E.; Reinhardt, H.W., Eds.; University of Michigan: Ann Arbor, **1995,** pp 139–182.
14. Møllmann, H. *Private communication;* **1995.**
15. *Beton-Bogen;* Herholdt, A.D.; Justesen, C.F.P.; Nepper-Christensen, P.; Nielsen, A., Eds.; Aalborg Portland, CTO, **1979,** p 354. (In Danish)
16. *Friction and Adhesion Tests: Butyl Sheeting Against Concrete etc,* Industrial Research Report 37/66; Department of Structural Engineering, Technical University of Denmark: Lyngby, **1967.**
17. Jensen, O.M. *Ph.D. Thesis;* Building Materials Laboratory, Technical University of Denmark: Lyngby, **1993.** (In Danish)
18. Bentur, A.; Mindess, S. *Fibre Reinforced Cementitious Composites;* Elsevier Applied Science: **1990.**
19. Bentur, A.; Odler, I. In *Interfacial Transition Zone in Concrete;* Maso, J.C., Ed.; Rilem Report 11, E&FN Spon: London, **1995,** pp 18–44.